Lysosomes targeting pH activable imaging-guided photodynamic agents

Carlotta Figliola, Halina Anton, Christophe Sutter, Camille Chériaux, Alexandra Sutter, Valérie Mazan, Mourad Elhabiri, Pascal Didier, Denis Jacquemin, Gilles Ulrich

ChemBioChem

Combining Chemistry and Biology

Chemistry Europe

European Chemical Societies Publishing

Accepted Article

Title: Lysosomes targeting pH activable imaging-guided photodynamic agents

Authors: Carlotta Figliola, Halina Anton, Christophe Sutter, Camille Chériaux, Alexandra Sutter, Valérie Mazan, Mourad Elhabiri, Pascal Didier, Denis Jacquemin, and Gilles Ulrich

To be cited as: *ChemBioChem* **2023**, e202300139

Link to VoR: https://doi.org/10.1002/cbic.202300139

WILEY-VCH

Lysosomes targeting pH activable imaging-guided photodynamic agents

Dr. Carlotta Figliola,*[a] Dr. Halina Anton,[b] Christophe Sutter,[a] Camille Chériaux,[a] Alexandra Sutter,[a] Dr. Valérie Mazan,[c] Dr. Mourad Elhabiri,[c] Prof. Dr. Pascal Didier,[b] Prof. Dr. Denis Jacquemin*[d,e] and Dr. Gilles Ulrich*[a]

[a] Institut de Chimie pour l'Energie, l'Environnement et la Santé (ICPEES), UMR CNRS 7515, Université de Strasbourg, 25 rue Becquerel, 67087 Strasbourg Cedex 02, France

[b] Laboratoire de Bioimagerie et Pathologies, UMR CNRS 7021, Faculté de Pharmacie, Université de Strasbourg, 74 Route du Rhin, 67401 Illkirch Cedex, France

[c] Laboratoire d'Innovation Moléculaire et Applications (LIMA), UMR CNRS 7042, Université de Strasbourg, 25 rue Becquerel, 67087 Strasbourg Cedex 02, France

[d] Nantes Université, CNRS, CEISAM UMR 6230, F-44000 Nantes, France

[e] Institut Universitaire de France (IUF), F-75005 Paris, France

corresponding authors e-mail: figliola@unistra.fr, denis.jacquemin@univ-nantes.fr, gulrich@unistra.fr

Abstract

Photodynamic therapy (PDT) is a photochemistry-based medical treatment combining light at a specific wavelength and a photosensitizer (PS) in the presence of oxygen. Application of PDT as a conventional treatment is limited and clearly the approval in clinics of new PS is challenging. The selective accumulation of the PS in the targeted malignant cells is of paramount importance to reduce the side effects that are typical of the current worldwide approved PS. Here we report a new series of aniline- and iodine-substituted BODIPY derivatives (**1-3**) as promising lysosome-targeting and pH-responsive theranostic PS, which displayed a significant *in vitro* light-induced cytotoxicity, efficient imaging properties and low dark toxicity (for **2** and **3**). These compounds were obtained in few reproducible synthetic steps and good yields. Spectroscopic and electrochemical measurements along with computational calculations confirmed the quenching of the emissive properties of the PS, while both fluorescence and $^1O_2$ emission were obtained only under acidic conditions inducing amine protonation. The pK_a values and pH-dependent emissive properties of **1-3** being established, their cellular uptake and activation in the lysosomal vesicles (pH ≈ 4-5) were confirmed by their co-localization with the commercial LysoTracker deep red and light-induced cytotoxicity (IC_{50} between 0.16 and 0.06 µM) against HeLa cancer cells.

Introduction

Photodynamic therapy (PDT) is a photochemistry-based medical treatment combining two non-toxic components, *i.e.*, light at a specific wavelength and a photosensitizer (PS).[1][2],[3],[4],[5] Owing to its minimal systematic invasiveness and dark toxicity,[6] PDT has been known for over 30 years as a promising anticancer and antimicrobial treatment.[1],[2],[3],[4],[5],[7] Upon light irradiation the PS reaches an excited singlet state (S_1), which undergoes intersystem crossing (ISC) populating the more stable and longer-lived excited triplet state (T_1). In the presence of molecular oxygen ($^3O_2$), the PS in its triplet state produces the reactive oxygen species (ROS, notably $OH^•$ and $O_2^{•-}$) by electron transfer as well as the singlet oxygen ($^1O_2$) by energy transfer.[3],[4],[5],[8] Both ROS and $^1O_2$ cause cell death by direct

disruption of cellular or microbial components (*e.g.,* membrane proteins and lipids, cellular organelles, nucleic acids, etc.) or, indirectly, by damaging the local vessels and inducing an inflammatory and immune response.[1],[3],[9]

Despite the development of many potential PS, only four PS have been approved worldwide (Photofrin®, Levulan®, Metvixia®, and Visudyne®) for treating superficial cancers, pre-cancerous lesions and age-related tissue degeneration.[4] Among them, Photofrin is still the most used in clinical trials although it lacks chemical purity and tissue selectivity, it shows weak red/near-infrared (NIR) light absorbance, it requires the use of high doses of drug and it causes skin hypersensitivity to sunlight for at least four weeks post-therapy.[10] The above-mentioned PS belong to the widespread family of porphyrins derivatives typically demanding time-consuming syntheses and purifications, while showing poor selectivity, low biocompatibility, and therapeutic efficiency.[2],[10-11] Indeed, clinical applications require the PS to absorb light in the red/NIR region, the so-called "therapeutic window", with a large molar absorptivity as well as to produce efficiently $^1O_2$.[4] Furthermore, it should be selective to the targeted tissue, but with high body clearance and water solubility, and it should not be toxic in the absence of light.[4] The partial selective accumulation of the above-mentioned PS is mostly dependent on the enhanced permeability and retention (EPR) effect of tumour cells (passive targeting). Active targeting *via* intracellular activation of the PS,[12],[13],[14],[15],[16],[17] or conjugation to a ligand binding an overexpressed receptor on malignant tissues[18],[19] have also been explored. However, to date, no preclinical or clinical advances of these two last strategies have been reported to the best of our knowledge.[3],[4] In addition, attention has also been focused on developing photodynamic theranostic systems enabling imaging diagnosis and simultaneous PDT.[20],[21],[22],[23],[24] When the imaging technique is based on fluorescence emission, the majority of these systems relies on a single molecule whose theranostic activity requires two simultaneous processes: fluorescence emission and $^1O_2$ generation.[8]

BODIPY-based PS have attracted tremendous attention in recent years because of their large extinction coefficients, high fluorescence quantum yields, chemical robustness, stability to light, solvents, and temperature variations.[25],[26],[27] Furthermore, their optical properties are easy to tune by synthetic modifications of the substituents on the dipyrromethene core reaching red/NIR emissions for biological imaging and sensing.[25],[26],[27] The popular strategy to promote the $^1O_2$ generation is the incorporation of heavy atoms, *e.g.,* transition metals and halogens enhancing the spin-orbit coupling strength and hence the ISC.[28],[29],[30],[31] The synthetic versatility of BODIPYs also allows to increase the selectivity towards the targeted tissues by conjugation to biomolecules for selective system delivery,[32],[33],[34],[35],[36],[37],[38] or by specific stimuli-responsive activation of the PS.[14],[15],[16] Indeed, the BODIPY molecular structure can be engineered with functional groups turning *on* or */off* specific spectroscopic signatures of molecules under specific physiological conditions and upon reaction with specific analytes allowing accumulation in targeted subcellular compartments, e.g., lysosomes,[39],[40],[41],[42], [43] lipidic membrane,[44],[45],[46], [47], [48] mitochondria,[43],[49],[50], [51],[52],[53],[54],[55],[56],[57] endoplasmic reticulum[43],[58] and nucleus.[59],[60],[61] More specifically, targeting the lysosomes is a known strategy to develop efficient anticancer therapeutics, including PDT agents, fluorescent probes and theranostic agents.[62],[63],[64],[65] Lysosomes is a polymorphic hydrolase-containing vesicles, which are responsible for the intracellular degradation and recycling pathways of proteins and other macromolecules.[62],[63],[64],[65] The well-functioning of lysosomes is strictly dependent on the integrity of its membrane, which, if disrupted in response to PDT, induces protons and hydrolases leakage into the cytoplasm and causes autophagy of the malignant cells.[3]

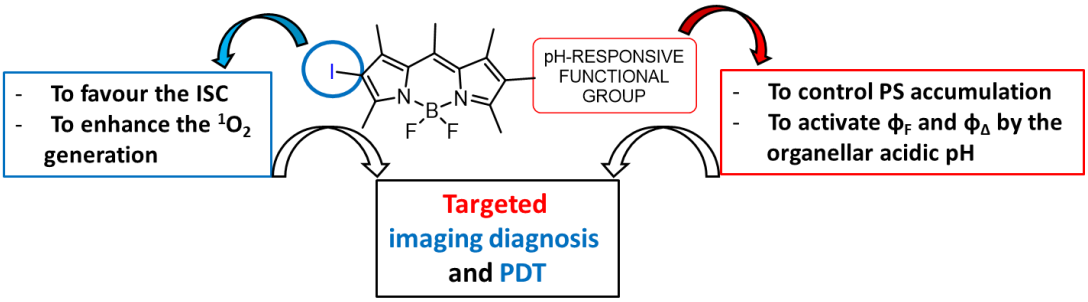

Figure 1. Lysosome-targeting pH-activable BODIPY-based theranostic agents.

Herein we report the design, the synthesis, and the characterization of a model series of lysosome-targeting pH-responsive theranostic PDT agents featuring a BODIPY core substituted in positions 2 and 6 with, on the one hand, an iodine atom to favour the ISC and hence enhance the $^1O_2$ generation and, on the other hand, a tertiary aniline as pH-responsive functional group (Figure 1). The advantage of using the pyrrolic position rather than the well-exploited *meso* one[40],[41],[66],[67] is to favour a mutually coaxial conformation between the two subunits (with or without a linker), which has been proved to efficiently tune the spectroscopic properties of the dyes, *via* intramolecular charge transfer (ICT) or photoinduced electron transfer (PeT).[68] Based on their pK_a values,[69],[70],[71] *N,N*-dialkylanilines have been previously used to prepare pH probes[71] and PDT agents[72],[40],[41] accumulating in cancerous lysosomes. The pK_a values of PS **1-3** are measured as well as both fluorescence emission and $^1O_2$ generation are explored and their efficiency determined. The mechanism by which the emissive properties of the reported PS **1-3** (structures in Scheme 1) are quenched and activated only under acidic conditions is investigated by spectroscopic and electrochemical studies as well as by theoretical calculations. Furthermore, the cellular uptake of PS **1-3** in HeLa cancer cells and, more specifically, in the lysosomal vesicles, where the activation of their emissive properties by the internal low pH (~4-5),[63] is confirmed by co-localization imaging experiments and photo-induced cytotoxicity.

Results and discussion

Synthesis

The new targeted pH-responsive theranostic agents **1-3** were synthetised from the 2,6-diiodo- and the 2-iodo-substituted BODIPY **4** and **6** (Scheme 1).[73] More specifically, compound **4** was reacted under Pd-catalysed Sonogashira reaction conditions to obtain directly **1** in 25% yield, while **6** gave compounds **8** and **10** *via* Suzuki and Stille cross-coupling in 66% and 60% yields, respectively. The final PS **2** and **3** were obtained in good yields (45% and 74%, respectively) by subsequent iodination of **8** and **10** with *N*-iodosuccinimide (NIS) (Scheme 1).

10.1002/cbic.202300139

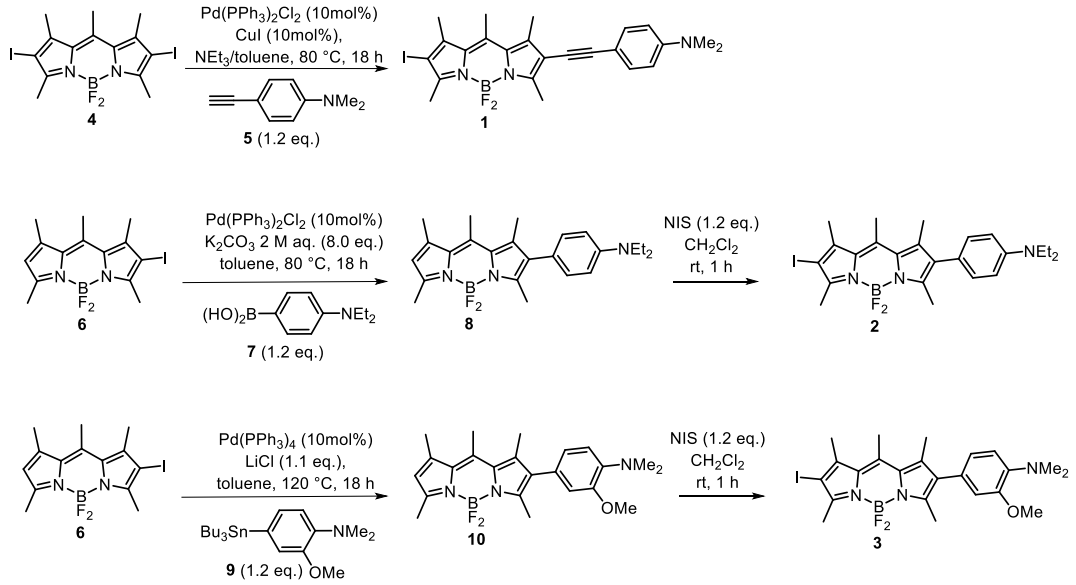

*Scheme 1. Synthesis of PS **1-3**.*

Photophysical characterization

The photophysical properties of PS **1-3** and their protonated species **1H-3H** were recorded at room temperature in different solvents (Table 1). As a general observation, the main absorption band of PS **1-3**, centred in the green region of the visible spectrum, corresponds to the S_0-S_1 transition and it is not well-structured but rather broad, indicating a sizeable ICT character. This is consistent with the presence of electron-donating group on the electron-acceptor BODIPY core,[26] which also induces a relatively small shift of the absorption maximum when the solvent polarity increases (see Table 1 and Figure 2, see also calculations below). Upon protonation of the amino group with HCl vapours, the corresponding PS **1H-3H** display, in all solvents, an increase of the molar absorption coefficient (ε) as well as a narrower absorption band with a hypsochromic shift of the maximum absorption band as compared to the non-protonated form (Figure 2). Again, a slight negative solvatochromism is observed (Table 1). Neutral PS **1** and **2** show a residual fluorescence emission in non-polar solvents *(i.e.*, *p*-xylene for both PS, toluene only for PS **2**). Increasing the polarity of the solvent (from CH_2Cl_2 to acetone) completely quenches the emission of **1** and **2**. In contrast, PS **3** does not emit in any of the tested solvents. Upon protonation fluorescence emission of compounds **1-3** is restored, with quantum yields (ϕ_F) between 7 and 12% (Table 1 and Supporting Information, SI). The insolubility of all protonated species in *p*-xylene and toluene (and in acetone for PS **1H**) does not allow obtaining the corresponding photophysical data (Table 1).

10.1002/cbic.202300139

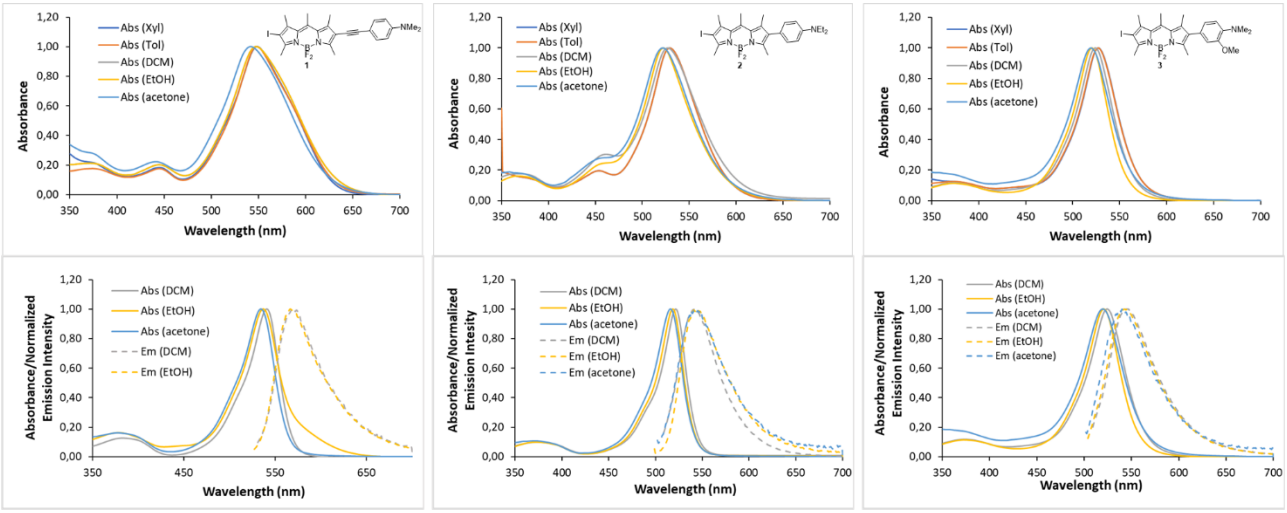

*Figure 2. Absorption spectra of PS **1-3** in solvents of different polarity (top), absorption and emission spectra of the corresponding protonated species **1H-3H** in polar solvents (bottom).*

The low values of ϕ_F are consistent with those of the parent compounds **4** and **6** and they can be explained by the halogen substitution of the BODIPY core enhancing the ISC channelling the excitation energy into the triplet state (T_1) and making these compounds poorly fluorescent.[73] The capability of PS **1-3** to generate $^1O_2$ was thus investigated using a protocol adapted from the literature (Table 1).[74] A solution of the PS, without and upon protonation with HCl vapours, and the 1,3-diphenylisobenzofuran (DPBF), as $^1O_2$ scavenger, in EtOH was irradiated at specific time intervals with a monochromator centred at 505 nm (see SI). The production of $^1O_2$ was calculated following the decrease of the maximum absorbance of the DBPF at 410 nm. The singlet oxygen quantum yields (ϕ_Δ) were then calculated as 44% (**1H**), 43% (**2H)** and 42% (**3H**, Table 1). The substitution of one iodine with tertiary anilines decreases the efficiency of the ISC because of a smaller spin-orbit coupling than the bis- and mono-iodo BODIPY derivative **4** and **6**, as confirmed by the theoretical calculation (see below). Indeed, compared to the two latter producing respectively $^1O_2$ in 87% and 64% quantum yields (see SI), the values are here lower. However, they are comparable to those reported for some bis-iodo BODIPY derivatives with (or without) quenching functional groups, considering the different experimental conditions.[40],[41],[51],[75],[76],[77] As expected, no $^1O_2$ production was observed in the absence of protonation of the amino groups (see SI).

Table 1. Optical spectroscopic data for compounds 1-3.

PS	solvent	λ_{abs} (nm)	ε ($M^{-1}\cdot cm^{-1}$)	λ_{em} (nm)	ΔSS (cm^{-1})	Φ_F (%)[a]	Φ_Δ (%)[b]	τ (ns)	k_r (s^{-1})	k_{nr} (s^{-1})
4[73]	CH_2Cl_2	527	9.0 x 10^4	548	727	6	87[b], 66[78],[c]	<1		
6[73]	CH_2Cl_2	509	9.0 x 10^4	529	743	14	64[b]	<1		
1	*p*-Xylene	552	2.4 x 10^4	663	3033	3		0.47	6.38 x 10^7	2.06 x 10^9
	toluene	550	3.2 x 10^4	n.d.						
	CH_2Cl_2	543	3.8 x 10^4	n.d.						
	EtOH	540	4.4 x 10^4	n.d.						
	acetone	536	2.1 x 10^4	n.d.						
1H[d]	CH_2Cl_2	545	6.6 x 10^4	569	842	12	n.d.	4.5	2.67 x 10^7	1.96 x 10^8
	EtOH	541	6.7 x 10^4	568	953	6	44	3.6	1.67 x 10^7	2.61 x 10^8
	acetone	535	3.7 x 10^4	n.d.			n.d.			
2	*p*-Xylene	532	2.6 x 10^4	673	4009	4		0.8	5.00 x 10^7	1.20 x 10^9

	toluene	530	2.7 x 10^4	669	3920	4		0.7	5.63 x 10^7	1.35 x 10^9
	CH_2Cl_2	527	4.8 x 10^4	n.d.						
	EtOH	522	5.2 x 10^4	n.d.						
	acetone	522	2.4 x 10^4	n.d.						
2H[d]	CH_2Cl_2	521	9.4 x 10^4	546	1093	7	n.d.	5.1	1.00 x 10^7	1.82 x 10^8
	EtOH	518	9.5 x 10^4	545	1051	9	43	5.3	1.70 x 10^7	1.72 x 10^8
	acetone	516	4.4 x 10^4	543	1027	12	n.d.	0.53	2.26 x 10^8	1.66 x 10^9
3	*p*-Xylene	527	3.1 x 10^4	n.d.						
	toluene	527	3.0 x 10^4	n.d.						
	CH_2Cl_2	524	5.9 x 10^4	n.d.						
	EtOH	520	6.4 x 10^4	n.d.						
	acetone	516	2.8 x 10^4	n.d.						
3H[d]	CH_2Cl_2	523	8.1 x 10^4	548	872	12	n.d.	0.5	2.40 x 10^8	1.75 x 10^9
	EtOH	518	8.2 x 10^4	546	876	10	42	0.5	2.00 x 10^8	1.80 x 10^9
	acetone	516	3.9 x 10^4	543	926	14	n.d.	0.7	2.06 x 10^8	1.26 x 10^9

[a] Φ_F were calculated by using Rhodamine 6G as a reference (λ_{exc} = 488 nm, Φ_F = 0.88 in EtOH); [b] Φ_Δ were obtained by using Rose Bengal as a reference (Φ_Δ = 0.76 in EtOH); [c]obtained by direct measurement of the singlet oxygen emission in CH_2Cl_2 and with (tetra-*tert*-butylphthalocyaninato)zinc(II) as reference;[78] [d]protonation was performed by bubbling HCl vapours in the solution containing PS **1-3**.

For closely related systems, the quenched fluorescence is explained by the presence of the electron-donating amino groups inducing an ICT at the excited state[79],[80],[81] or a reductive PeT,[39],[40],[67],[82],[49] or sometimes the quenching mechanism is not described.[83],[84] Concerning PS **1** and **2**, the residual fluorescence emission in non-polar solvents suggests that the ICT could be considered as the responsible mechanism for quenching the emission in polar solvents and in the absence of protonation. However, the same reasoning is not valid for PS **3** since this dye is non-emissive in *p*-xylene and toluene. The feasibility of the reductive electron transfer from the HOMO of the substituent to the LUMO of the BODIPY core depends on the reducing potential of the PS **1-3** and the oxidation potential of the tertiary anilines.[25] Consequently, cyclic voltammetry on the PS **1-3** was performed (Table 2 and SI).

*Table 2. Electrochemical data of PS **1-3**.*

PS	$E_{red}(A/A^{\bullet-})$[a] (V vs Fc/Fc^+)	$E_{ox\text{-}1}(D^{\bullet+}/D)$[b] (V vs Fc/Fc^+)	$E_{ox\text{-}2}(A^{\bullet+}/A)$[b] (V vs Fc/Fc^+)	$E_{0,0}$[c] (eV)	$\Delta G_{(PeT)}$[d] (eV)
1	-1.19	0.70	1.28	1.97	-0.08
2	-1.26	0.72	1.10	2.07	-0.09
3	-1.27	0.67	1.02	2.19	-0.25

Cyclic voltammetry was carried out in deoxygenated CH_2Cl_2 solutions, containing 0.1 M $TBAPF_6$, at a solute concentration of 1.0-1.5 mM, at a scan rate of 100 V s^{-1} and at 25 °C. Potentials were standardized using ferrocene (Fc) as internal reference and converted to SCE assuming that $E_{1/2}$ (Fc/Fc^+) = +0.38 V (vs SCE). [a] $E_{red}(A/A^{\bullet-})$ is defined as the reduction potential of A (acceptor); [b] $E_{ox\text{-}1}(D^{\bullet+}/D)$ is defined as the oxidation potential of D (donor); [c] $E_{0,0}$ is defined as the excited state energy of the dye and approximated as the interception of the tangent of absorption band on its descending side with the wavelength axis; [d] $\Delta G_{(PeT)} = -(E_{ox\text{-}1}(D^{\bullet+}/D) - E_{red}(A/A^{\bullet-})) - E_{0,0} - w$, w describes the coulombic impact of the charge separation depending on the solvent dielectric constant ($w \sim 1/\varepsilon$) is generally omitted.[85]

All the voltammograms of the reported systems are characterized by a reversible reduction wave in the range of -1.30 V and -1.20 V corresponding to π-radical anion of the BODIPY core and two reversible oxidation waves consistent with the radical cation of the tertiary amine (around 0.70 V) and of the

BODIPY (in the range of 1.00 V and 1.30 V).[26],[86],[87] As expected, protonation of the mesomeric electron-donating group impedes the oxidation of the tertiary amino group and the reductive PeT to occur. Indeed, the voltammograms of the corresponding **1H-3H** do not show the first reversible oxidation wave matching with the oxidation of the amino group. Based on these measurements, the free energy of the PeT process ($\Delta G_{(PeT)}$) was estimated to be -0.08 (**1**), -0.09 (**2**) and -0.25 (**3**) eV using the Rehm-Weller equation.[25] Concerning PS **1** and **2**, the experimental $\Delta G_{(PeT)}$ values could suggest that both the reductive PeT and the ICT are involved in quenching their emissive properties. In respect of PS **3**, a reductive PeT is the most likely quenching mechanism.

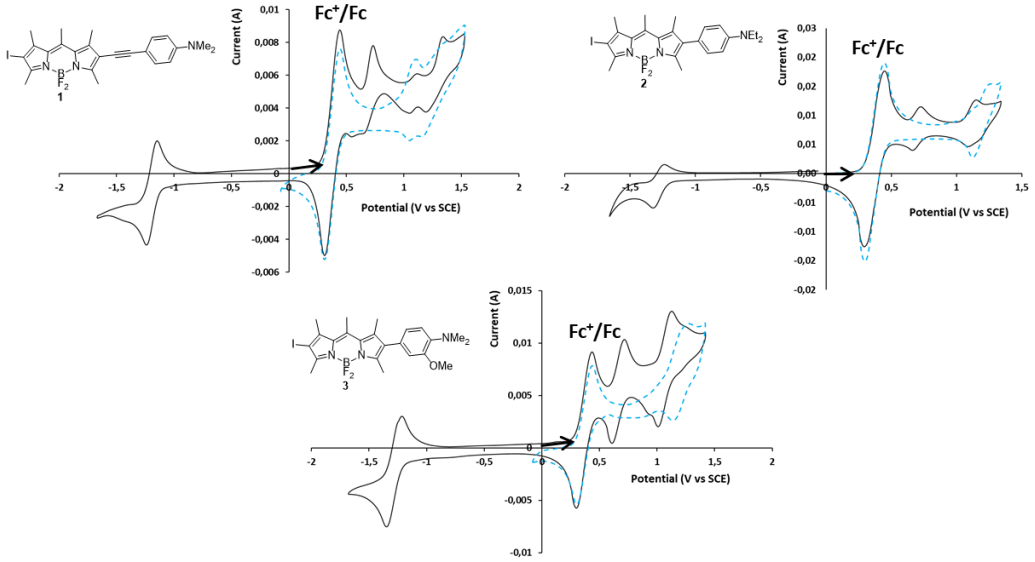

*Figure 3. Cyclic voltammetry of PS **1-3** (black solid line) and of their protonated forms **1H-3H** (blue dashed line).*

The presence of an ICT process, even if weak (Table 1 and Figure 2), prompted us to study the two-photon absorption (TPA) properties of PS **1-3** after protonation to assess the possibility of using them as theranostic TPA-PS. Indeed, the two-photon irradiation combined with the pH-dependent PS activation can ensure the optimal light penetration, the selectivity, and the accuracy in controlling the $^1O_2$ production. TPA cross-section spectra of protonated PS **1H-3H** using Rhodamine B as a reference[88] were measured in EtOH using a tuneable femtosecond laser (120 fs pulses in the 680–1300 nm spectral range; Figure 4, left). PS **1H-3H** display two absorption bands centred at λ=775 and 1000 nm with relatively low TPA cross-section (in the range of 2-18 GM and 1-4 GM for the 775 and 1000 nm bands, respectively), compared to similar literature systems. Integrated fluorescence intensities were measured by exciting at 760 and 900 nm as a function of the applied laser power and the results confirmed a good correlation of the fluorescence emission intensity with the square of the applied excitation intensity (Figure 4, right). However, based on the low values of the cross-section, the reported series of compounds **1-3** could not be used as efficient 2PA-PS; however, the good ϕ_Δ along with the residual fluorescent emission (Table 1) allow studying them as potential theranostic one-photon absorption PDT agents.

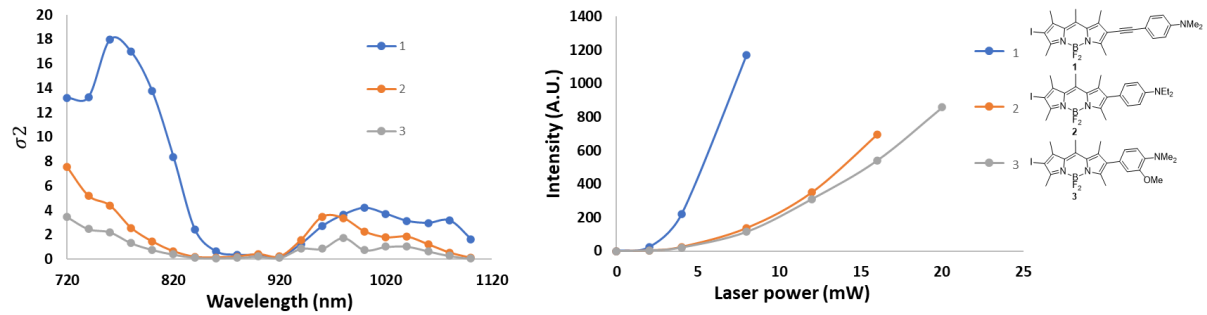

*Figure 4. (Left) TPA cross-section spectrum of PS **1H-3H** measured in EtOH, with an average laser power of 0.5 mW; (right) correlation of the fluorescence emission intensity with the square of the power intensity at 840 nm.*

Due to their hydrophobic nature, PS **1-3** are insoluble in water. Consequently, to perform pH titration of the tertiary anilines and measure the corresponding pK_a values, PS **1-3** were encapsulated in the non-ionic surfactant Cremophor EL® (see the SI for details), extensively used in pharmaceutical applications. pH-Titrations clearly demonstrate that protonation of PS **2-3** under weak acidic conditions results in a significant hyperchromic shift of the S_0-S_1 transitions concomitant to a weak bathochromic shift in agreement with the spectroscopic data collected in various organic solvents (Table 1). For PS **2**, a pK_a value of 2.60 ± 0.08 has been measured. As a consequence of the mesomeric effect of the *ortho*-methoxy with respect to the dimethylamino unit, a higher pK_a value (3.64 ± 0.08) has been determined for PS **3** (Figure S 13). For PS **1** containing a dimethylaniline, the pK_a value was estimated to be < 2 (Figure S 11). According to these values, we could suggest that PS will be mainly protonated (PS **3**) or partially protonated (PS **1** and **2**) and thus activated in the cellular lysosomes (see below).

Theoretical calculations have been performed to obtain additional insights into the properties of the synthesized PS systems (see the SI for technical details). Figure 5 shows the electron density difference (EDD) plots for neutral and protonated PS. These EDDs show that the BODIPY core act as an electron acceptor (mostly in red), whereas the side groups act as donor (mostly in blue), confirming the ICT. The latter effect is, as expected, decreased when the amino groups are protonated. One can also note on Figure 5, that the contribution of the iodine centre in the excited state is notably increased after protonation.

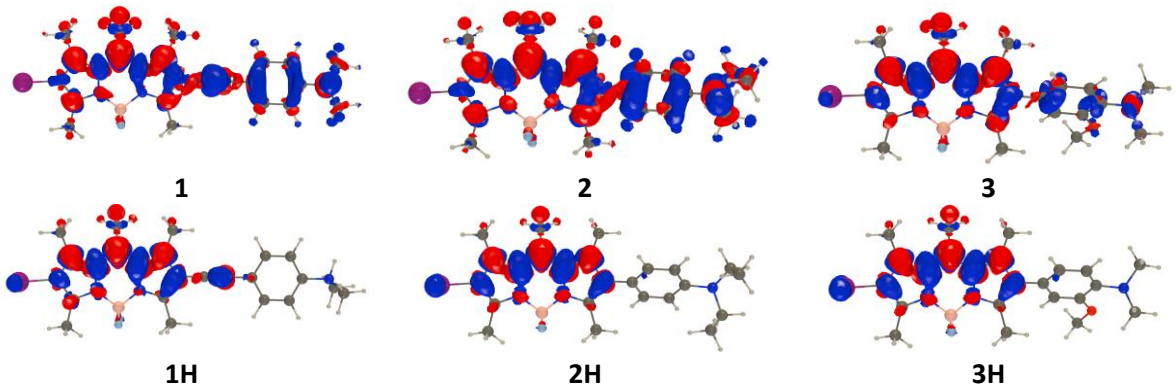

Figure 5. Density difference plots for the considered systems. Navy blue and crimson red lobes correspond to decrease and increase of density upon excitation (threshold 0.001 au). All calculations are made in DCM.

In Table S1 in the SI, we provide vertical absorption and emission energies, as well as the 0-0 energies, the latter being directly comparable to the experimental absorption-fluorescence crossing points for emissive dyes. For the vertical emission, theory predicts significant blueshifts upon protonation (-159 nm for **1**, -202 nm for **2**, and -252 nm for **3**), values that are in line with experiment (-94 nm for **1**, and -127 nm for **2**). For the 0-0 energies, the theoretical protocol provides a mean absolute error with respect to experiment of 0.11 eV, confirming the quality of the selected level of theory.

The above noted ICT can be quantified using the well-known Le Bahers' index, which provides an ICT distance (d^{CT}). The d^{CT} values are 4.45 Å, 3.60 Å, and 1.46 Å, for **1**, **2**, and **3**, respectively. The large values for the two former PS **1** and **2** are consistent with fluorescence quenching by ICT, whereas the smaller d^{CT} for PS **3**, is consistent with the twisting of the dimethylamino group induced by the presence of a vicinal methoxy moiety (see Figure 5). Upon protonation, all these values decrease significantly and attain 1.01 Å, 0.41 Å, and 0.86 Å. Further, to estimate the possibility of PeT in the neutral **1-3**, we

have compared the total energies of the optimal ICT S_1 and the corresponding charged-separated (CS) structures, the latter being determined by constrained-DFT in which a +1/-1 charge was enforced on the phenyl-amino/BODIPY moieties, respectively. Both structures have been optimized and their final energies compared. In **1** and **2**, we found that the CS structure is less stable by 0.43 and 0.30 eV, respectively. This indicates that PeT is very unlikely in both **1** and **2**. In contrast, the two structures have alike energies for **3** (Δ=0.09 eV, within the error bar of the selected level of theory), hinting that PeT might be possible in this structure. Though, due to the inherent approximations of the various schemes, these values are not equivalent to the experimental ones, the joint analysis of theoretical and measured data allow to safely conclude that ICT is the dominant quenching mechanism in both **1** and **2**; whereas PeT is the dominant non-radiative pathway for **3**. For the records, we also investigated the possibility of TICT in **1-3**. To this end, we started excited state optimizations from structures in which the $NAlk_2$ or the Ph-$NAlk_2$ were orthogonally positioned with respect to the core of the dye, but these minimizations led back to the standard minimum, indicating that TICT is not a major non-deactivation path in these PS.

We have also investigated the ISC considering that it occurs from the relaxed S_1 geometry. Our data are listed in the SI. In all systems, there is only one triplet state accessible from this geometry, with S_1-T_1 gaps ranging from 0.28 to 0.61 eV, the values being smaller in **1-3**, than in **4-6** and **1H-3H**. What is more interesting are the amplitudes of the spin-orbit couplings matrix elements (SOCME) that are relatively smaller than one wavenumber for **1** (0.18 cm^{-1}), **2** (0.39 cm^{-1}), and **3** (0.66 cm^{-1}), but significantly higher for all other systems: **1H** (0.78 cm^{-1}), **2H** (1.16 cm^{-1}), **3H** (1.18 cm^{-1}), **4** (1.67 cm^{-1}), and **6** (1.00 cm^{-1}). These significant enlargements are consistent with the EDDs of Figure 5 and the experimental trends showing enhanced formation of $^1O_2$ after protonation.

Biological tests

Once the pH-dependent emissive properties of PS **1-3** were established, preliminary biological *in vitro* tests were performed. First, co-localization experiments were run to determine their accumulation and activation in the cellular digestive organelles with an acidic intravesicular pH (~4-5).

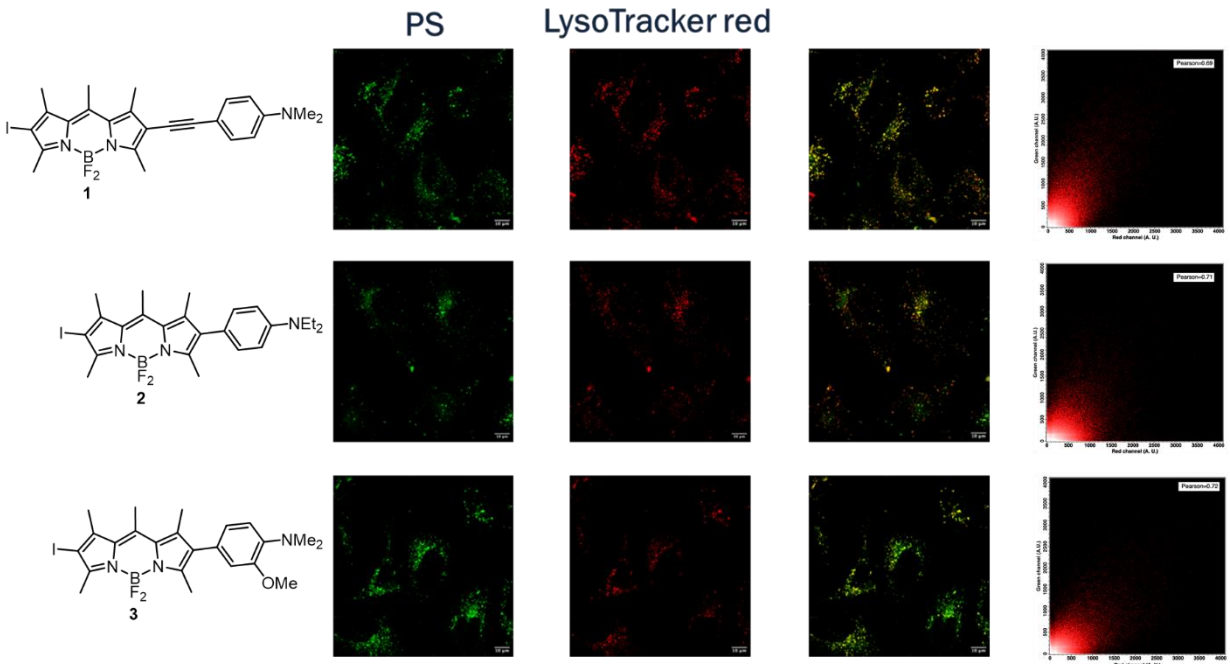

*Figure 5. CLSM obtained with live HeLa cells stained with the Cremophor EL-encapsulated PS **1-3** and Lyso Tracker deep red in PBS buffer; (far right) scatter plot of red and green pixel intensity of HeLa cells.*

As previously mentioned, due to its intrinsic hydrophobic nature, PS **1-3** are insoluble in pure water or PBS buffer solution (pH = 7.4). Consequently, they were again encapsulated in the Cremophor EL® ensuring a good solubility in PBS buffer solution (see SI for details). Subsequently, HeLa cancer cells were incubated for 15 minutes with the freshly prepared assembly of **1-3** along with the commercial dye LysoTracker deep red and imaged using confocal laser scanning microscopy (CLSM), as shown in Figure 5. In addition, Pearson correlation coefficients of 0.69 (**1**), 0.71 (**2**) and 0.72 (**3**) confirm that the three PS are accumulated well in the cells, they all localize in the cytosol and more specifically in the acidic vesicles (Figure 5). Based on the latter, the the imaging properties in Hela cells of all three dyes is consistent with their accumulation in the lysosomes (lysosomotropic action) due to partial protonation and according to pK_a values estimated in the potentiometric conditions.[89],[90],[91] This underlines the difficulty to translate the experimental conditions used for the evaluation of pK_a values to the cellular lysosome environment.

The cytotoxicity of PS **1-3** was tested by MTT based cell viability assay. HeLa cells were incubated in presence of varying concentrations of the Cremophor EL®-encapsulated PS **1-3** for 30 minutes, after which cells were washed with PBS to remove all the non-internalized molecules and put in complete culture medium (see the SI). Next, the samples were irradiated using LED light at 505 nm with a low light dose (power density = 0.42mW/cm^2) during 2 and 6 hours in the incubator. Following the irradiation, the cells were incubated in the dark for additional 14 hours to allow the damaged cells to trigger the apoptotic response. At the end of this period the fraction of viable cells was measured by MTT assay. After 2 hours of irradiation the cell viability remains 20%, while after 6 hours it reaches less than 10% (Figure 6). PS **1**, **2**, and **3** showed efficient phototoxicity with good IC_{50} of 0.16 µM, 0.12 µM and 0.12 µM, respectively. Next, we performed the same experiments with a higher light power density (power density = 7.1mW/cm²) and for shorter irradiation times (Figure 6). The IC_{50} values measured for the three PS are summarized in Table 3. The increase of the light power density is linearly correlated to the cytotoxicity efficiency of PS **2**, but not for PS **3**, which remains unvaried. In contrast to **2** and **3**, which have been proved promising theranostic agents, PS **1** showed an important dark cytotoxicity. The mechanism, following which **1** is toxic to cells even in the absence of light, is currently under investigation.

*Table 3. Correlation between the light power density and the efficiency of phototoxicity of PS **1-3**.*

	IC_{50} after 6 h at PD = 0.42mW/cm²	**IC_{50} after 5 min, PD = 7.1mW/cm²**	**IC_{50} after 10 min, PD = 7.1mW/cm²**
1	0.16 µM	0.16 µM	0.14 µM
2	0.12 µM	0.08 µM	0.06 µM
3	0.12 µM	0.24 µM	0.12 µM

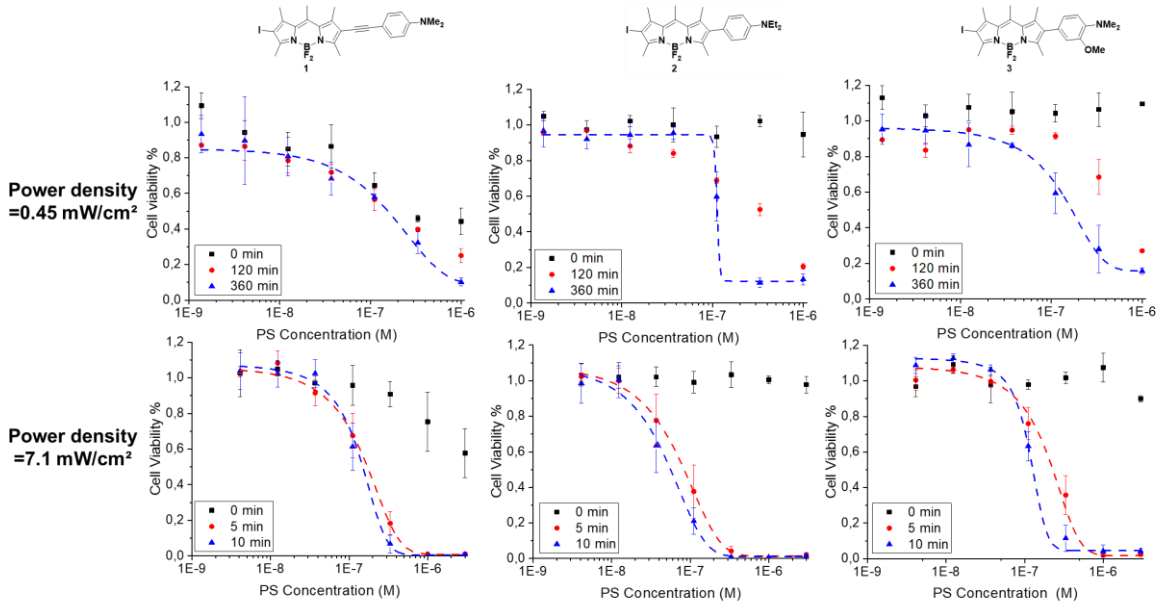

*Figure 6. Cell viability after 6 hours irradiation followed by 14 hours incubation in presence of **PS 1-3** (red squares) and in the absence of light (black squares). All experiments were performed twice with triplicate sample for each condition. The error bars correspond to the average of the absolute deviation for each data set.*

Conclusions

In conclusion, we have developed a new series of lysosome-targeting pH-activable BODIPY-based theranostic as to favour the selective accumulation of the PDT agents and $^1O_2$ production in defined cellular compartments. The synthetically straightforward substitution of the BODIPY core with an iodine and a dialkyl tertiary aniline allows the $^1O_2$ generation and the acidic pH-responsive emissive behaviour, respectively. A detailed analysis of the physico-chemical and photophysical properties of the reported BODIPY derivatives was performed by means of pH-titration, spectroscopic and electrochemical analyses as well as theoretical calculations. We have determined both ϕ_F and ϕ_Δ, demonstrated the dependence of the PS emissive properties on the pH of the surrounding environment and investigated which mechanisms, ICT or reductive PeT, are involved in quenching both fluorescence and $^1O_2$ emission of the non-protonated forms. Exploiting the Cremophor EL®-encapsulation helping the water solubility of hydrophobic molecules, the pH-activable properties of this series of compounds have been further verified by biological *in vitro* experiments. The cellular uptake, accumulation, and activation in the lysosomal vesicles of HeLa cancer cells have been confirmed by optimal co-localization imaging experiments and photo-induced toxicity with low dark toxicity (the latter for PS **2** and **3**). We intend to further extend this series of PS as to shift the absorption and emission spectra in the therapeutic window, to improve both their biocompatibility and their selectivity towards malignant tissues. The present work paves the way to an efficient strategy for designing smart theranostic agents for more efficient PDT therapy.

Author contributions

C. F. performed the synthesis, conducted the spectroscopic and electrochemical characterization, and prepared the original draft. H. A. performed the *in vitro* photo-induced cytotoxic tests. C. S. provided the irradiation system used for the *in vitro* photo-induced cytotoxic tests. C. C. and A. S. conducted supplementary spectroscopic experiments. P. D. performed the measurements of the 2PA cross section and the CLSM experiments. D. J. performed the theoretical calculations. V. M. performed the absorption *versus* pH measurements. M. E. analysed and determined the pK_a values of

photosensitizers. G.U. supervised and revised the manuscript. All authors have approved the final version of the manuscript.

Conflicts of interest

There are no conflicts to declare.

Acknowledgments

C. F. thanks the Interdisciplinary Institute HiFunMat for support of the SMARTY starting grant. This work of the Interdisciplinary Institute HiFunMat, as part of the ITI 2021–2028 program of the University of Strasbourg, CNRS and Inserm, was supported by IdEx Unistra (ANR-10-IDEX-0002) and SFRI (STRAT'US project, ANR-20-SFRI-0012) under the framework of the French Investments for the Future Program. Furthermore, C. F. thanks the CNRS for additional financial support. D.J. thanks the CCIPL/GliCiD computational centre for generous allocation of computational time.

Keywords

BODIPYs, intraorganellar activation, photodynamic therapy, pH-responsive photosensitizers, selectivity

References

[1] D. E. J. G. J. Dolmans, D. Fukumura, R. K. Jain, *Nat. Rev. Cancer* **2003**, *3*, 380-387.
[2] H. Abrahamse, M. R. Hamblin, *Biochem. J.* **2016**, *473*, 347-364.
[3] D. Van Straten, V. Mashayekhi, S. H. De Bruijn, S. Oliveira, J. D. Robinson, *Cancers* **2017**, *9*, 19-73.
[4] S. Monro, K. L. Colón, H. Yin, J. Roque, P. Konda, S. Gujar, R. P. Thummel, L. Lilge, C. G. Cameron, S. A. McFarland, *Chem. Rev.* **2019**, *119*, 797-828.
[5] T. C. Pham, V.-N. Nguyen, Y. Choi, S. Lee, J. Yoon, *Chem. Rev.* **2021**, *121*, 13454-13619.
[6] J. Dobson, G. F. De Queiroz, J. P. Golding, *Vet. J.* **2018**, *233*, 8-18.
[7] G. B. Kharkwal, S. K. Sharma, Y.-Y. Huang, T. Dai, M. R. Hamblin, *Lasers Surg. Med.* **2011**, *43*, 755-767.
[8] J. P. Celli, B. Q. Spring, I. Rizvi, C. L. Evans, K. S. Samkoe, S. Verma, B. W. Pogue, T. Hasan, *Chem. Rev.* **2010**, *110*, 2795-2838.
[9] Q. Xiao, B. Mai, Y. Nie, C. Yuan, M. Xiang, Z. Shi, J. Wu, W. Leung, C. Xu, S. Q. Yao, P. Wang, L. Gao, *ACS Appl. Mater. Interfaces* **2021**, *13*, 11588-11596.
[10] A. E. O'Connor, W. M. Gallagher, A. T. Byrne, *Photochem. Photobiol.* **2009**, *85*, 1053-1074.
[11] K. Plaetzer, B. Krammer, J. Berlanda, F. Berr, T. Kiesslich, *Lasers Med. Sci.* **2009**, *24*, 259-268.
[12] E. Kozma, P. Kele, *Org. Biomol. Chem.* **2019**, *17*, 215-233.
[13] M. H. Lee, A. Sharma, M. J. Chang, J. Lee, S. Son, J. L. Sessler, C. Kang, J. S. Kim, *Chem. Soc. Rev.* **2018**, *47*, 28-52.
[14] S. Callaghan, M. O. Senge, *Photochem. Photobiol. Sci.* **2018**, *17*, 1490-1514.
[15] X. Li, S. Kolemen, J. Yoon, E. U. Akkaya, *Adv. Funct. Mater.* **2017**, *27*, 1604053-1604064.
[16] J. F. Lovell, T. W. B. Liu, J. Chen, G. Zheng, *Chem. Rev.* **2010**, *110*, 2839-2857.
[17] Q. Xiao, H. Lin, J. Wu, X. Pang, Q. Zhou, Y. Jiang, P. Wang, W. Leung, H. Lee, S. Jiang, S. Q. Yao, L. Gao, G. Liu, C. Xu, *J. Med. Chem.* **2020**.
[18] J. Sandland, R. W. Boyle, *Bioconjugate Chem.* **2019**, *30*, 975-993.
[19] M. Srinivasarao, P. S. Low, *Chem. Rev.* **2017**, *117*, 12133-12164.
[20] M. Lan, S. Zhao, W. Liu, C.-S. Lee, W. Zhang, P. Wang, *Adv. Healthc. Mat.* **2019**, *8*, 1900132-1900169.
[21] X. Zhao, J. Liu, J. Fan, H. Chao, X. Peng, *Chem. Soc. Rev.* **2021**, *50*, 4185-4219.
[22] J. Li, K. Pu, *Chem. Soc. Rev.* **2019**, *48*, 38-71.

[23] S. Jenni, A. Sour, *Inorganics* **2019**, *7*, 10-23.
[24] R. Kumar, W. S. Shin, K. Sunwoo, W. Y. Kim, S. Koo, S. Bhuniya, J. S. Kim, *Chem. Soc. Rev.* **2015**, *44*, 6670-6683.
[25] A. Loudet, K. Burgess, *Chem. Rev.* **2007**, *107*, 4891-4932.
[26] G. Ulrich, R. Ziessel, A. Harriman, *Angew. Chem. Int. Ed.* **2008**, *47*, 1184-1201.
[27] N. Boens, B. Verbelen, M. J. Ortiz, L. Jiao, W. Dehaen, *Coord. Chem. Rev.* **2019**, *399*, 213024-.
[28] aS. G. Awuah, Y. You, *RSC Adv.* **2012**, *2*, 11169-11183; bT. Yogo, Y. Urano, Y. Ishitsuka, F. Maniwa, T. Nagano, *J. Am. Chem. Soc.* **2005**, *127*, 12162-12163.
[29] A. Kamkaew, S. H. Lim, H. B. Lee, L. V. Kiew, L. Y. Chung, K. Burgess, *Chem. Soc. Rev.* **2013**, *42*, 77-88.
[30] J. Zhao, K. Xu, W. Yang, Z. Wang, F. Zhong, *Chem. Soc. Rev.* **2015**, *44*, 8904-8939.
[31] E. Bassan, A. Gualandi, P. G. Cozzi, P. Ceroni, *Chem. Sci.* **2021**, *12*, 6607-6628.
[32] S.-l. Niu, C. Massif, G. Ulrich, P.-Y. Renard, A. Romieu, R. Ziessel, *Chem. Eur. J.* **2012**, *18*, 7229-7242.
[33] S. Osati, H. Ali, J. E. v. Lier, *J. Porphyr. Phthalocyanines* **2016**, *20*, 61-75.
[34] S. J. Scales, S. P. Tsai, N. Zacharias, J. D. Cruz-Chuh, G. Bullen, E. Velasquez, J. Chang, E. Bruguera, K. R. Kozak, J. Sadowsky, *Bioconjugate Chem.* **2019**, *30*, 3046-3056.
[35] I. Bacsa, C. Konc, A. Orosz, G. Kecskeméti, R. Rigó, C. Özvegy-Laczka, E. Mernyák, *Molecules* **2018**, *23*, 821.
[36] S. Karan, M. Y. Cho, H. Lee, H. Lee, H. S. Park, M. Sundararajan, J. L. Sessler, K. S. Hong, *J. Med. Chem.* **2021**.
[37] aJ. Chavda, K. Bhavsar, S. Gupta, I. Gupta, *J. Porphyr. Phthalocyanines* **2021**, *25*, 1230-1239; bA. Turksoy, D. Yildiz, E. U. Akkaya, *Coord. Chem. Rev.* **2019**, *379*, 47-64.
[38] E. Antina, N. Bumagina, Y. Marfin, G. Guseva, L. Nikitina, D. Sbytov, F. Telegin, *Molecules* **2022**, *27*, 1396.
[39] S. O. McDonnell, M. J. Hall, L. T. Allen, A. Byrne, W. M. Gallagher, D. F. O'Shea, *J. Am. Chem. Soc.* **2005**, *127*, 16360-16361.
[40] F. Xue, P. Wei, X. Ge, Y. Zhong, C. Cao, D. Yu, T. Yi, *Dyes Pigm.* **2018**, *156*, 285-290.
[41] H. Xiong, K. Zhou, Y. Yan, J. B. Miller, D. J. Siegwart, *ACS Appl. Mater. Interfaces* **2018**, *10*, 16335-16343.
[42] M. Li, R. Tian, J. Fan, J. Du, S. Long, X. Peng, *Dyes Pigm.* **2017**, *147*, 99-105.
[43] D. Kand, L. Pizarro, I. Angel, A. Avni, D. Friedmann-Morvinski, R. Weinstain, *Angew. Chem. Int. Ed.* **2019**, *58*, 4659-4663.
[44] A. S. Klymchenko, *Acc. Chem. Res.* **2023**, *56*, 1-12.
[45] T. Mukherjee, R. J. Martinez-Sanchez, K. T. Fam, S. Bou, L. Richert, D. Garnier, Y. Mély, S. Kanvah, A. S. Klymchenko, M. Collot, *Mater. Chem. Front.* **2021**, *5*, 2459-2469.
[46] L. Michels, V. Gorelova, Y. Harnvanichvech, J. W. Borst, B. Albada, D. Weijers, J. Sprakel, *PNAS* **2020**, *117*, 18110-18118.
[47] D. O' Connor, A. Byrne, T. E. Keyes, *RSC Adv.* **2019**, *9*, 22805-22816.
[48] D. Listunov, S. Mazères, Y. Volovenko, E. Joly, Y. Génisson, V. Maraval, R. Chauvin, *Bioorg. Med. Chem. Lett.* **2015**, *25*, 4652-4656.
[49] S. Qi, N. Kwon, Y. Yim, V.-N. Nguyen, J. Yoon, *Chem. Sci.* **2020**.
[50] R. He, Y. Zhang, S. Madhu, Q. Gao, Q. Lian, S. S. Raghavan, J. Geng, *Chem. Commun.* **2020**, *56*, 14717-14720.
[51] U. Bhattacharyya, B. K. Verma, R. Saha, N. Mukherjee, M. K. Raza, S. Sahoo, P. Kondaiah, A. R. Chakravarty, *ACS Omega* **2020**, *5*, 4282-4292.
[52] R. Tiwari, P. S. Shinde, S. Sreedharan, A. K. Dey, K. A. Vallis, S. B. Mhaske, S. K. Pramanik, A. Das, *Chem. Sci.* **2021**, *12*, 2667-2673.
[53] A. Garai, I. Pant, A. Bhattacharyya, P. Kondaiah, A. R. Chakravarty, *ChemistrySelect* **2017**, 11686-11692.
[54] H. Chen, X. He, M. Su, W. Zhai, H. Zhang, C. Li, *J. Am. Chem. Soc.* **2017**, *139*, 10157-10163.
[55] X. Feng, T. Zhang, J.-T. Liu, J.-Y. Miao, B.-X. Zhao, *Chem. Commun.* **2016**, *52*, 3131-3134.

[56] X. Kong, F. Su, L. Zhang, J. Yaron, F. Lee, Z. Shi, Y. Tian, D. R. Meldrum, *Angew. Chem. Int. Ed.* **2015**, *54*, 12053-12057.

[57] J.-T. Hou, K. Li, J. Yang, K.-K. Yu, Y.-X. Liao, Y.-Z. Ran, Y.-H. Liu, X.-D. Zhou, X.-Q. Yu, *Chem. Commun.* **2015**, *51*, 6781-6784.

[58] Y. He, J. Shin, W. Gong, P. Das, J. Qu, Z. Yang, W. Liu, C. Kang, J. Qu, J. S. Kim, *Chem. Commun.* **2019**, *55*, 2453-2456.

[59] H. Huang, O. Starodub, A. McIntosh, A. B. Kier, F. Schroeder, *J. Biol. Chem.* **2002**, *277*, 29139-29151.

[60] A. Nakamura, K. Takigawa, Y. Kurishita, K. Kuwata, M. Ishida, Y. Shimoda, I. Hamachi, S. Tsukiji, *Chem. Commun.* **2014**, *50*, 6149-6152.

[61] Z. Lv, Y. Wang, J. Zhang, Z. Wang, G. Jin, *J. Mol. Struc.* **2021**, *1234*, 130201.

[62] Z. Guo, S. Park, J. Yoon, I. Shin, *Chem. Soc. Rev.* **2014**, *43*, 16-29.

[63] W. Xu, Z. Zeng, J.-H. Jiang, Y.-T. Chang, L. Yuan, *Angew. Chem. Int. Ed.* **2016**, *55*, 13658-13699.

[64] J. Yin, Y. Hu, J. Yoon, *Chem. Soc. Rev.* **2015**, *44*, 4619-4644.

[65] N.-E. Choi, J.-Y. Lee, E.-C. Park, J.-H. Lee, J. Lee, *Molecules* **2021**, *26*, 217.

[66] S. Radunz, S. Wedepohl, M. Röhr, M. Calderón, H. R. Tschiche, U. Resch-Genger, *J. Med. Chem.* **2020**, *63*, 1699-1708.

[67] Y. Urano, D. Asanuma, Y. Hama, Y. Koyama, T. Barrett, M. Kamiya, T. Nagano, T. Watanabe, A. Hasegawa, P. L. Choyke, H. Kobayashi, *Nat. Med.* **2009**, *15*, 104-109.

[68] T. G. Kim, J. C. Castro, A. Loudet, J. G. S. Jiao, R. M. Hochstrasser, K. Burgess, M. R. Topp, *J. Phys. Chem.* **2006**, *110*, 20-27.

[69] Perrin, D.D. (1965) Dissociation Constants of Organic Bases in Aqueous Solution. Butterworths, London (Supplement, 1972).

[70] A. N. Pankratov, I. M. Uchaeva, S. Y. Doronin, R. K. Chernova, *J. Struct. Chem.* **2001**, *42*, 739-746.

[71] A. Sutter, M. Elhabiri, G. Ulrich, *Chem. Eur. J.* **2018**, *24*, 11119-11130.

[72] H. Horiuchi, A. Hirabara, T. Okutsu, *J. Photochem. Photobiol. Chem.* **2018**, *365*, 60-66.

[73] L. Bonardi, G. Ulrich, R. Ziessel, *Org. Lett.* **2008**, *10*, 2183-2186.

[74] H. Savoie, C. Figliola, E. Marchal, B. W. Crabbe, G. L. Hallett-Tapley, R. W. Boyle, A. Thompson, *Photochem. Photobiol. Sci.* **2018**, *17*, 599-606.

[75] P. Hu, X. L. Weng, C. H. Zhu, D. C. Yang, J. Y. Liu, Z. Chen, M. Huang, *ChemPlusChem* **2022**, *87*, e202200158.

[76] G. Linden, L. Zhang, F. Pieck, U. Linne, D. Kosenkov, R. Tonner, O. Vázquez, *Angew. Chem. Int. Ed.* **2019**, *58*, 12868-12873.

[77] S. H. Lim, C. Thivierge, P. Nowak-Sliwinska, J. Han, H. Van Den Bergh, G. WagnièRes, K. Burgess, H. B. Lee, *J. Med. Chem.* **2010**, *53*, 2865-2874.

[78] Y. P. Rey, D. G. Abradelo, N. Santschi, C. A. Strassert, R. Gilmour, *Eur. J. Org. Chem.* **2017**, *2017*, 2170-2178.

[79] M. Obłoza, Ł. Łapok, T. Pędziński, K. M. Stadnicka, M. Nowakowska, *ChemPhysChem* **2019**, *20*, 2482-2497.

[80] H. Horiuchi, A. Hirabara, T. Okutsu, *J. Photochem. Photobiol. A* **2018**, *365*, 60-66.

[81] H. Horiuchi, R. Kuribara, A. Hirabara, T. Okutsu, *J. Phys. Chem. A* **2016**, *120*, 5554-5561.

[82] T. Werner, C. Huber, S. Heinl, M. Kollmannsberger, J. Daub, O. S. Wolfbeis, *Fresenius' J. Anal. Chem.* **1997**, *359*, 150-154.

[83] X.-D. Jiang, L. Jia, Y. Su, C. Li, C. Sun, L. Xiao, *Tetrahedron* **2019**, *75*, 4556-4560.

[84] W. Lin, W. Zhang, S. Liu, Z. Li, X. Hu, Z. Xie, C. Duan, G. Han, *ACS Appl. Mater. Interfaces* **2019**, *11*, 43928-43935.

[85] N. A. Romero, D. A. Nicewicz, *Chem. Rev.* **2016**, *116*, 10075-10166.

[86] W.-J. Shi, P.-C. Lo, A. Singh, I. Ledoux-Rak, D. K. P. Ng, *Tetrahedron* **2012**, *68*, 8712-8718.

[87] S. Niu, G. Ulrich, P. Retailleau, R. Ziessel, *Tetrahedron Lett.* **2011**, *52*, 4848-4853.

[88] S. E. El Meshri, E. Boutant, A. Mouhand, A. Thomas, V. Larue, L. Richert, V. Vivet-Boudou, Y. Mély, C. Tisné, D. Muriaux, H. de Rocquigny, *Biochim. Biophys. Acta Gen. Subj.* **2018**, *1862*, 1421-1431.
[89] M. Zhu, P. Xing, Y. Zhou, L. Gong, J. Zhang, D. Qi, Y. Bian, H. Du, J. Jiang, *J. Mat. Chem. B* **2018**, *6*, 4422-4426.
[90] Y. Zhang, H.-M. Fang, X.-T. Zhang, S. Wang, G.-W. Xing, *ChemistrySelect* **2016**, *1*, 1-6.
[91] L. Yang, J.-Y. Niu, R. Sun, Y.-J. Xu, J.-F. Ge, *Org. Biomol. Chem.* **2017**, *15*, 8402-8409.

10.1002/cbic.202300139

Table of Contents

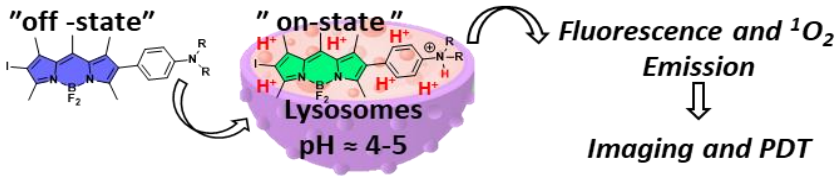

The potential photodynamic activity of prototypical acidic pH-responsive BODIPYs targeting cellular lysosomes have been demonstrated by a comprehensive study going from the synthesis to the biological evaluation and including photophysical and theoretical studies. It provides an efficient strategy to design smart theranostic agents for more selective and efficient photodynamic PDT.

Personal and institutional Twitter handles:
@carlotta_figl
@icpees
@CNRS_Alsace